THREE-STEP EXPLICIT FINITE ELEMENT COMPUTATION OF SHALLOW WATER FLOWS ON A MASSIVELY PARALLEL COMPUTER

KAZUO KASHIYAMA AND HANAE ITO

Department of Civil Engineering, Chuo University, 1-13-27 Kasuga, Bunkyo-ku, Tokyo 112, Japan

AND

MAREK BEHR AND TAYFUN TEZDUYAR

AEM/AHPCRC, Supercomputer Institute, University of Minnesota, 1200 Washington Avenue South, Minneapolis, MN55415, U.S.A.

SUMMARY

Massively parallel finite element strategies for large-scale computations of shallow water flows and contaminant transport are presented. The finite element discretizations, carried out on unstructured grids, are based on a three-step explicit formulation both for the shallow water equations and for the advection–diffusion equation governing the contaminant transport. Parallel implementations of these unstructured-grid-based formulations are carried out on the Army High Performance Computing Research Center Connection Machine CM-5. It is demonstrated with numerical examples that the strategies presented are applicable to large-scale computations of various shallow water flow problems.

KEY WORDS: three-step explicit scheme; parallel computing; shallow water flow; tidal flow; Tokyo Bay

INTRODUCTION

Finite element computations of shallow water flows and contaminant transport can be applied to many practical problems: design of river, coastal and offshore structures, disaster prediction and other applications related to hydrodynamic, thermal and chemical transport behaviour in oceans, lakes and rivers. In this context the finite element method is applicable to complicated water and land configurations. In practical computations of this type of problem it is essential to use methods which are as efficient and fast as the available hardware allows. Also, computations need to be carried out over long time durations to properly simulate and predict the phenomena of interest.

In recent years, massively parallel finite element computations have been successfully applied to several large-scale flow problems.[1–3] These computations demonstrated the availability of a new level of finite element computational capability to solve practical flow problems. With the need for a high-performance computing environment to carry out simulations for practical problems in shallow water flows and contaminant transport, in this paper we present and employ a parallel explicit finite element method for computations based on unstructured grids. The finite element discretizations are based on a three-step explicit formulation both for the shallow water equations and for the advection–diffusion equation governing the contaminant transport. In these discretizations, for numerical stabilization, we use selective lumping[4,5] for the shallow water equations and the streamline upwind/Petrov–Galerkin (SUPG) technique[6,7] for the advection–diffusion equation. The three-node linear triangular element is

used for all variables. Parallel implementation of these unstructured-grid-based formulations are carried out on the Connection Machine CM-5. In order to show the efficiency of the three-step scheme, the computed results are compared with the results obtained by the conventional two-step scheme.[4,5] As a real-life test problem we carry out simulations of the effect of the tidal current on Tokyo Bay and the spread of a pollutant introduced in the bay.

GOVERNING EQUATIONS

The governing equations of shallow water flow are

$$\frac{\partial U_i}{\partial t} + U_j U_{i,j} + g\zeta_{,i} + \frac{\tau_i^b}{\rho(h+\zeta)} - A_l(U_{i,j} + U_{j,i})_{,j} + f_i = 0, \tag{1}$$

$$\frac{\partial \zeta}{\partial t} + [(h+\zeta)U_j]_{,j} = 0, \tag{2}$$

where $\mathbf{U}$ is the mean horizontal velocity, ζ is the water elevation, h is the water depth, g is the gravitational acceleration, A_l is the eddy viscosity and $\mathbf{f}$ is the Coriolis force. The bottom friction τ_i^b can be given as

$$\tau_i^b = \frac{n^2 g}{h^{1/3}} U_i (U_k U_k)^{1/2}, \tag{3}$$

where n is the Manning coefficient. The Coriolis force can be given as $f_1 = -kU_2, f_2 = kU_1$, where k denotes the Coriolis acceleration.

Transport of contaminant, on the other hand, is governed by the advection–diffusion equation

$$\frac{\partial \phi}{\partial t} + (\phi U_j)_{,j} - \kappa \phi_{,jj} = 0, \tag{4}$$

where ϕ is the concentration, $\mathbf{U}$ is the current velocity and κ is the diffusion coefficient.

SPATIAL AND TEMPORAL DISCRETIZATION

For the finite element spatial discretization of the governing equations the selective lumping Galerkin[4,5] and SUPG[6,7] methods are used for the shallow water and advection–diffusion equations respectively. The weak form of the governing equations can then be written as

$$\int_\Omega W_i(U_{i,t} + U_j U_{i,j} + g\zeta_{,i} + \frac{\tau_i^b}{p(h+\zeta)} + f_i)\mathrm{d}\Omega + \int_\Omega W_{i,j} A_l(U_{i,j} + U_{j,i})\mathrm{d}\Omega = \int_\Gamma W_i t_i \mathrm{d}\Gamma = 0, \tag{5}$$

$$\int_\Omega \xi\{\zeta_{,t} + [(h+\zeta)U_j]_{,j}\}\mathrm{d}\Omega = 0, \tag{6}$$

$$\int_\Omega \varphi[\phi_{,t} + (U_j\phi)_{,j}]\mathrm{d}\Omega + \int_\Omega \varphi_{,j}\kappa\phi_{,j}\mathrm{d}\Omega + \sum_{e=1}^{N_{el}} \int_{\Omega_e} \tau U_j\varphi_{,j}[\phi_{,t} + (U_j\phi)_{,j} - \kappa\phi_{,jj}]\mathrm{d}\Omega - \int_\Gamma \varphi q \mathrm{d}\Gamma = 0, \tag{7}$$

where $\mathbf{W}$, ξ and φ denote weighting functions, τ is the SUPG stabilization parameter and t_i and q are given boundary terms.

Using the three-node linear triangular element for the spatial discretization, the following finite element equations can be obtained:

$$M_{\alpha\beta}U_{\beta i,t} + K_{\alpha\beta\gamma j}U_{\beta j}U_{\gamma i} + H_{\alpha\beta i}\zeta_\beta + E_{\alpha\beta}U_{\beta i} + T_{\beta i} + S_{\alpha i\beta j}U_{\beta j} = 0, \tag{8}$$

$$M_{\alpha\beta}\zeta_{\beta t} + B_{\alpha\beta j\gamma}U_{\beta j}(h_\gamma + \zeta_\gamma) + C_{\alpha\beta\gamma j}U_{\beta j}(h_\gamma + \zeta_\gamma) = 0, \tag{9}$$

$$M_{\alpha\beta}^* \phi_{\beta,t} + B_{\alpha\beta j\gamma}^* \phi_\beta U_{\gamma j} + C_{\alpha\beta\gamma j}^* \phi_\beta U_{\gamma j} + D_{\alpha j\beta j}\phi_\beta = 0, \tag{10}$$

where

$$M_{\alpha\beta}^* = M_{\alpha\beta} + M_{\alpha\beta}^\delta, \qquad B_{\alpha\beta j\gamma}^* = B_{\alpha\beta j\gamma} + B_{\alpha\beta j\gamma}^\delta, \qquad C_{\alpha\beta\gamma j}^* = C_{\alpha\beta\gamma j} + C_{\alpha\beta\gamma j}^\delta \tag{11}$$

and superscript δ denotes the SUPG contribution. The bottom friction term is linearized and the water depth is interpolated using linear interpolation.

For discretization in time the three-step explicit time integration scheme is employed[8] using the Taylor series expansion

$$f(t + \Delta t) = f(t) + \Delta t \frac{\partial f(t)}{\partial t} + \frac{\Delta t^2}{2}\frac{\partial^2 f(t)}{\partial t^2} + \frac{\Delta t^3}{6}\frac{\partial^3 f(t)}{\partial t^3} + O(\Delta t^4), \tag{12}$$

where f is an arbitrary function and Δt is the time increment. Using the approximate equation up to third-order accuracy, the following three-step scheme can be obtained:

first step

$$f\left(t + \frac{\Delta t}{3}\right) = f(t) + \frac{\Delta t}{3}\frac{\partial f(t)}{\partial t}, \tag{13a}$$

second step

$$f\left(t + \frac{\Delta t}{2}\right) = f(t) + \frac{\Delta t}{2}\frac{\partial f(t + \Delta t/3)}{\partial t}, \tag{13b}$$

third step

$$f(t + \Delta t) = f(t) + \Delta t \frac{\partial f(t + \Delta t/2)}{\partial t}. \tag{13c}$$

Equations (13) are equivalent to equation (12) and the method is referred to as the three-step Taylor–Galerkin method. This method has third-order accuracy for linear differential equations and second-order accuracy for non-linear differential equations.[9] Applying this procedure to the governing equations, the following discretized equations in time can be obtained:

first step

$$M_{\alpha\beta}^L U_{\beta i}^{n+1/3} = M_{\alpha\beta}^L U_{\beta i}^n - \frac{\Delta t}{3}(K_{\alpha\beta\gamma j}U_{\beta j}^n U_{\gamma i}^n + H_{\alpha\beta i}\zeta_\beta^n + E_{\alpha\beta}U_{\beta i}^n + T_{\beta i}^n + S_{\alpha i\beta j}U_{\beta j}^n), \tag{14a}$$

$$M_{\alpha\beta}^L \zeta_\beta^{n+1/3} = M_{\alpha\beta}^S \zeta_\beta^n - \frac{\Delta t}{3}[B_{\alpha\beta j\gamma}U_{\beta j}^n(h_\gamma + \zeta_\gamma^n) + C_{\alpha\beta\gamma j}U_{\beta j}^n(h_\gamma + \zeta_\gamma^n)], \tag{14b}$$

$$M_{\alpha\beta}^{*L} \phi_\beta^{n+1/3} = M_{\alpha\beta}^{*L} \phi_\beta^n - \frac{\Delta t}{3}(B_{\alpha\beta j\gamma}^* \phi_\beta^n U_{\gamma j}^{n+1/3} + C_{\alpha\beta\gamma j}^* \phi_\beta^n U_{\gamma j}^n + D_{\alpha j\beta j}\phi_\beta^n), \tag{14c}$$

second step

$$M_{\alpha\beta}^{\mathrm{L}} U_{\beta i}^{n+1/2} = M_{\alpha\beta}^{\mathrm{L}} U_{\beta i}^{n} - \frac{\Delta t}{2} (K_{\alpha\beta\gamma j} U_{\beta j}^{n+1/3} U_{\gamma i}^{n+1/3} + H_{\alpha\beta i}\zeta_{\beta}^{n+1/3} + E_{\alpha\beta} U_{\beta i}^{n+1/3} + T_{\beta i}^{n+1/3} + S_{\alpha i\beta j} U_{\beta j}^{n+1/3}),$$

(15a)

$$M_{\alpha\beta}^{\mathrm{L}} \zeta_{\beta}^{n+1/2} = M_{\alpha\beta}^{\mathrm{S}} \zeta_{\beta}^{n} - \frac{\Delta t}{2} [B_{\alpha\beta j\gamma} U_{\beta j}^{n+1/3}(h_{\gamma} + \zeta_{\gamma}^{n+1/3}) + C_{\alpha\beta\gamma j} U_{\beta j}^{n+1/3}(h_{\gamma} + \zeta_{\gamma}^{n+1/3})],$$

(15b)

$$M_{\alpha\beta}^{*\mathrm{L}} \phi_{\beta}^{n+1/2} = M_{\alpha\beta}^{*\mathrm{L}} \phi_{\beta}^{n} - \frac{\Delta t}{2} (B_{\alpha\beta j\gamma}^{*} \phi_{\beta}^{n+1/3} U_{\gamma j}^{n+1/3} + C_{\alpha\beta\gamma j}^{*} \phi_{\beta}^{n+1/3} U_{\gamma j}^{n+1/3} + D_{\alpha j\beta j} \phi_{\beta}^{n+1/3}),$$

(15c)

third step

$$M_{\alpha\beta}^{\mathrm{L}} U_{\beta i}^{n+1} = M_{\alpha\beta}^{\mathrm{L}} U_{\beta i}^{n} - \Delta t (K_{\alpha\beta\gamma j} U_{\beta j}^{n+1/2} U_{\gamma i}^{n+1/2} + H_{\alpha\beta i}\zeta_{\beta}^{n+1/2} + E_{\alpha\beta} U_{\beta i}^{n+1/2} + T_{\beta i}^{n+1/2} + S_{\alpha i\beta j} U_{\beta j}^{n+1/2}),$$

(16a)

$$M_{\alpha\beta}^{\mathrm{L}} \zeta_{\beta}^{n+1} = M_{\alpha\beta}^{\mathrm{S}} \zeta_{\beta}^{n} - \Delta t [B_{\alpha\beta j\gamma} U_{\beta j}^{n+1/2}(h_{\gamma} + \zeta_{\gamma}^{n+1/2}) + C_{\alpha\beta\gamma j} U_{\beta j}^{n+1/2}(h_{\gamma} + \zeta_{\gamma}^{n+1/2})],$$

(16b)

$$M_{\alpha\beta}^{*\mathrm{L}} \phi_{\beta}^{n+1} = M_{\alpha\beta}^{*\mathrm{L}} \phi_{\beta}^{n} - \Delta t (B_{\alpha\beta j\gamma}^{*} \phi_{\beta}^{n+1/2} U_{\gamma j}^{n+1/2} + C_{\alpha\beta\gamma j}^{*} \phi_{\beta}^{n+1/2} U_{\gamma j}^{n+1/2} + D_{\alpha j\beta j} \phi_{\beta}^{n+1/2}),$$

(16c)

where superscript n denotes the value computed at the nth time point and Δt is the time increment between the nth and $(n + 1)$th time steps. The coefficient $M_{\alpha\beta}^{\mathrm{L}}$ expresses the lumped coefficient and $M_{\alpha\beta}^{\mathrm{S}}$ is the selective lumping coefficient

$$M_{\alpha\beta}^{\mathrm{S}} = eM\alpha\beta^{\mathrm{L}} + (1 - e)M_{\alpha\beta},$$

(17)

where e the selective lumping parameter.

STABILITY ANALYSIS

The CFL stability condition for the one-dimensional linear shallow water equation is investigated. The basic equation is written as

$$\frac{\partial U}{\partial t} + g\zeta_{,x} = 0,$$

(18)

$$\frac{\partial \zeta}{\partial t} + hU_{,x} = 0,$$

(19)

where U is the velocity, ζ is the water elevation, g is the gravitational acceleration and h is the water depth. The water depth is assumed for simplicity to be constant over the whole domain. The two-node linear element is used for the spatial discretization and the three-step explicit scheme is employed for the numerical integration in time. The discretized equations for the ith nodal point can be written as follows:

first step

$$U_i^{n+1/3} = \frac{1-e}{6} U_{i-1}^{n} + \frac{2+e}{3} U_i^{n} + \frac{1-e}{6} U_{i+1}^{n} - g\frac{\mu}{3}(-\tfrac{1}{2}\zeta_{i-1}^{n} + \tfrac{1}{2}\zeta_{i+1}^{n}),$$

(20)

$$\zeta_i^{n+1/3} = \frac{1-e}{6} \zeta_{i-1}^{n} + \frac{2+e}{3} \zeta_i^{n} + \frac{1-e}{6} \zeta_{i+1}^{n} - h\frac{\mu}{3}(-\tfrac{1}{2} U_{i-1}^{n} + \tfrac{1}{2} U_{i+1}^{n}),$$

(21)

second step

$$U_i^{n+1/2} = \frac{1-e}{6} U_{i-1}^n + \frac{2+e}{3} U_i^n + \frac{1-e}{6} U_{i+1}^n - g\frac{\mu}{2}\left(-\tfrac{1}{2}\zeta_{i-1}^{n+1/3} + \tfrac{1}{2}\zeta_{i+1}^{n+1/3}\right), \qquad (22)$$

$$\zeta_i^{n+1/2} = \frac{1-e}{6} \zeta_{i-1}^n + \frac{2+e}{3} \zeta_i^n + \frac{1-e}{6} \zeta_{i+1}^n - h\frac{\mu}{2}(-\tfrac{1}{2} U_{i-1}^{n+1/3} + \tfrac{1}{2} U_{i+1}^{n+1/3}), \qquad (23)$$

third step

$$U_i^{n+1} = \frac{1-e}{6} U_{i-1}^n + \frac{2+e}{3} U_i^n + \frac{1-e}{6} U_{i+1}^n - g\mu(-\tfrac{1}{2}\zeta_{i-1}^{n+1/2} + \tfrac{1}{2}\zeta_{i+1}^{n+1/2}), \qquad (24)$$

$$\zeta_i^{n+1} = \frac{1-e}{6} \zeta_{i-1}^n + \frac{2+e}{3} \zeta_i^n + \frac{1-e}{6} \zeta_{i+1}^n - h\mu(-\tfrac{1}{2} U_{i-1}^{n+1/2} + \tfrac{1}{2} U_{i+1}^{n+1/2}), \qquad (25)$$

where

$$\mu = \frac{\Delta t}{\Delta x}. \qquad (26)$$

Consider the solution of the type

$$U_i^n = R^n \exp(j\omega i), \qquad (27)$$

$$\zeta_i^n = S^n \exp(j\omega i), \qquad (28)$$

where $j = \sqrt{(-1)}$ and R and S are the amplification factors of velocity and water elevation respectively. Introducing equations (27) and (28) into equations (20)–(25) and rearranging the terms, the following equation can be derived:

$$\begin{bmatrix} R^{n+1/3} \\ S^{n+1/3} \\ R^{n+1/2} \\ S^{n+1/2} \\ R^{n+1} \\ S^{n+1} \end{bmatrix} = \begin{bmatrix} a & \tfrac{1}{3}gb & & & & \\ \tfrac{1}{3}hb & a & & & & \\ a & & & \tfrac{1}{2}gb & & \\ & & a & \tfrac{1}{2}hb & & \\ a & & & & & gb \\ & & a & & & hb \end{bmatrix} \begin{bmatrix} R^n \\ S^n \\ R^{n+1/3} \\ S^{n+1/3} \\ R^{n+1/2} \\ S^{n+1/2} \end{bmatrix}, \qquad (29)$$

where

$$a = \frac{2+e}{3} - \frac{1-e}{3}\cos\omega, \qquad b = -j\mu\sin\omega.$$

The CFL stability condition can be obtained from equation (29) by using the fact that the eigenvalues of the coefficient matrix should be less than unity:

$$\mu = \frac{\Delta t}{\Delta x} \leqslant \left(\frac{3}{gh}\right)^{1/2} (1-e)^{1/2}. \qquad (30)$$

The stability limit is 1·5 times larger than that of the conventional two-step scheme.[4]

PARALLEL IMPLEMENTATION

The data-parallel implementation has been carried out on the Connection Machine CM-5. For the implementation, two types of data arrays at element level and equation level are used. The element-level arrays store the data with one element and its degrees of freedom associated with exactly one virtual processor. On the other hand, the equation-level arrays keep variables at the level of the global equation system. The nodal data, co-ordinates, element-level properties and element-level matrix and vectors are stored in arrays of element-level type. The global increment variables are kept in an array of equation-level type. Figure 1 shows the data storage modes.[2] Communication operation from equation level to element level is called a gather, while movement of the data from element level to equation level is called a scatter. Both gather and scatter may be implemented efficiently on the Connection Machine computer. In order to save communication time, the mesh-partitioning[3] feature of the Connection Machine Scientific Software Library (CMSSL) is used.

The discretized element-level equation can be expressed as

$$(M^{L}_{\alpha\beta})_e(x_\beta)_e = (f_\beta)_e, \tag{31}$$

where $(M^{L}_{\alpha\beta})_e$ is the element-level lumped mass matrix, $(x_\beta)_e$ is the element-level unknown vector and $(f_\beta)_e$ is the element-level known vector. The computation of the element-level lumped mass matrix and the element-level known vector is performed at the element level. Then these values are assembled at the equation level by a scatter operation. The unknown variables x_β are solved by

$$x_\beta = f_\beta / M^{L}_{\alpha\beta} \tag{32}$$

and the boundary conditions are imposed at the equation level. Figure 2 shows the structure of the finite element programme for the time step loop. In this figure n denotes the time step.
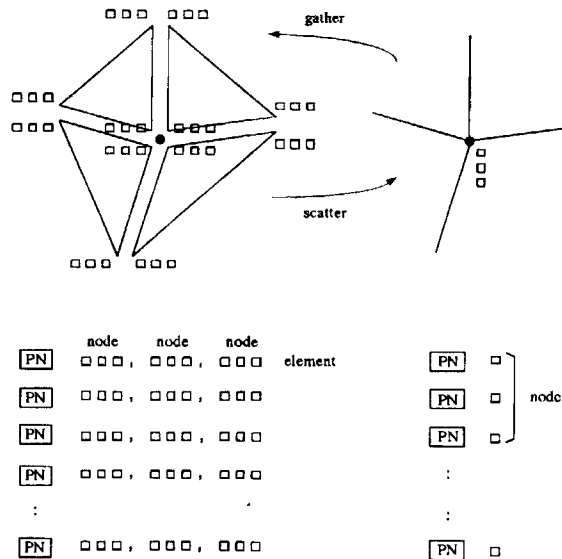

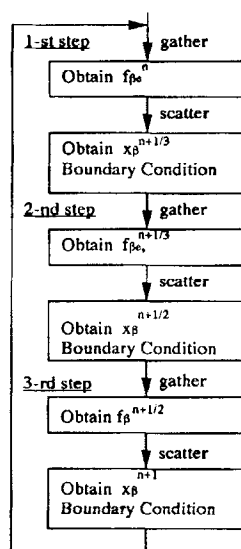Figure 1. Element-level (left) and equation-level (right)

Figure 2. Structure of time step loop

NUMERICAL EXAMPLES

In order to show the efficiency of the three-step scheme, the finite element analysis for the one-dimensional wave propagation problem is considered and the computed results are compared with the results obtained by the conventional two-step scheme. Figure 3 shows the finite element discretization and boundary conditions. The numbers of elements and nodes are 500 and 378 respectively. In this computation the fluid is assumed to be a perfect fluid and the water depth is assumed to be 10 m. For the boundary conditions the incident wave amplitude and wave period are assumed to be 1·0 m and 5 s respectively. The selective lumping parameter and time increment are assumed to be 0·9 and 0·006 s respectively. Figure 4 shows the computed water elevation at $t = 30$ s. In this figure the full curve represents the computed results obtained by the three-step scheme and the broken curve represents the computed results obtained by the two-step scheme. It can be seen that the computed results are in good agreement. Figure 5 shows the computed maximum water elevation for the first 30 s. In this figure the broken line at 1 m represents the exact value. It can be seen that unstable phenomena are obtained around the inlet boundary in the case of the two-step scheme (broken curve), while the computed results obtained by the three-step scheme (full curve) are close to the exact value.

As a real-life numerical example, simulation of tidal flow and contaminant transport in Tokyo Bay is carried out. In the past, several numerical results on the tidal current in Tokyo Bay have been presented.[10–12] However, conventional studies have not accounted for the configuration of geometrical boundary and water depth accurately, since a coarse mesh was used in the computations. The aim of this study is to determine the details of the flow pattern of the tidal current in Tokyo Bay. Figure 6 shows the configuration of the boundary and water depth diagram of Tokyo Bay. The water depth contours are evenly spaced between 5 m and 100 m at 5 m intervals, while the maximum depth is 545 m. In this computation a fine mesh which represents the geometry accurately is employed. Figure 7 shows the finite element discretization of Tokyo Bay. The total numbers of elements and nodes are 207,797 and 107,282 respectively. This mesh is designed to keep the element Courant number constant over the entire domain.[13,14] It can be seen that an appropriate mesh in accordance with the variation in water depth can be obtained. For the boundary condition the incident wave elevation is specified on the open boundary A–B as $\zeta = a \sin(2\pi t/T)$, where a is the incident wave amplitude, T is the incident wave
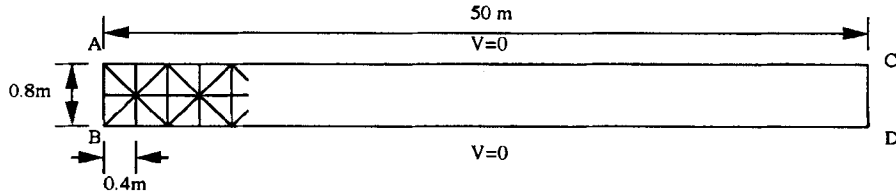
Figure 3. Finite element discretization. Boundary condition $\zeta = a \sin(2\pi t/T)$ on A–B, $U = \zeta \sqrt{(g/(h + \zeta))}$ on A–B, C–D
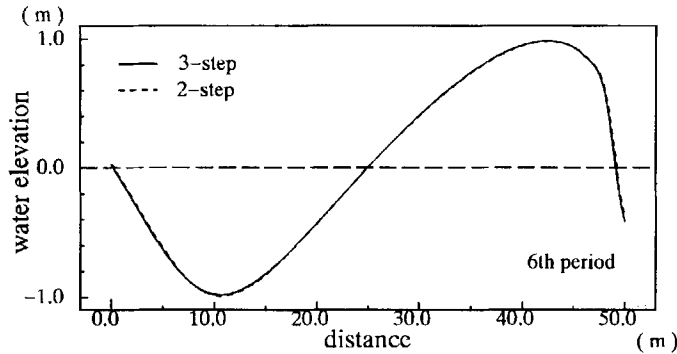

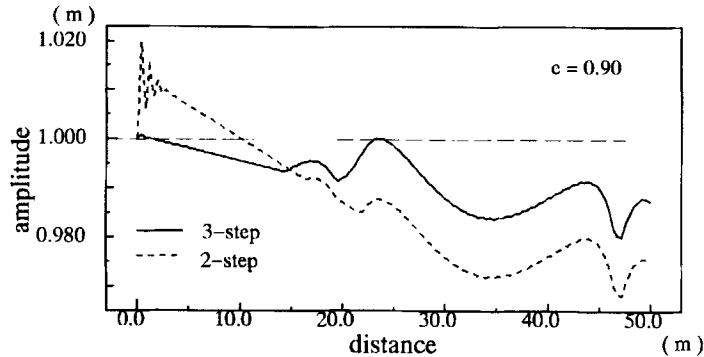Figure 4. Computed water elevation at $t = 30$ s

Figure 5. Computed maximum wave amplitude

period and t denotes time. The incident wave period is assumed to be 12·42 h (M$_2$ tide) and the incident wave amplitude is assumed to be 0·36 m.[15,16] The non-slip boundary condition is used on boundaries. The computation is started from the state of still water. For the numerical condition the following data are used: $A_t = 5$ m^2 s^{-1}, $n = 0·03$ and $\kappa = 5$ m^2 s^{-1}. Figure 8 shows the mesh partitioning for 1024 vector units. Figures 9 and 10 show respectively the water depth diagram and finite element discretization of the Uraga–Suido channel where the configuration of water depth is highly complicated. Figures 11 and 12 show the computed current velocity distribution around Uraga–Suido at high tide ($t = 43·470$ h) and low tide ($t = 49·680$ h) respectively. Figure 13 shows the computed residual flow and Figure 14 shows the streamline of the residual flow. From the latter figure it can be seen that some small vortices exist around the Uraga–Suido channel. For the contaminant transport analysis the concentration is given at point P (see Figure 10) as an initial condition. Figure 15
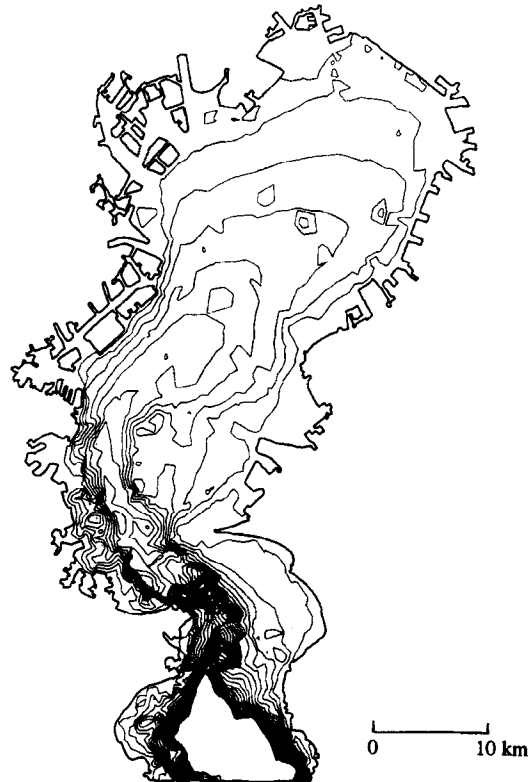
Figure 6. Boundary and water depth diagram of Tokyo Bay

shows the contaminant spread at every 3·105 h interval. It can be seen that the contaminant is spread in accordance with the periodic oscillation due to the tidal current. The computational speed using 1024 vector units is 0·340 s/step and 3·16 ms/step/node.

CONCLUSIONS

A three-step explicit finite element solver has been presented and implemented on a massively parallel supercomputer. The method has been applied to several problems and the computed results are compared with the results obtained by the conventional two-step scheme. The conclusions derived are as follows.

1. The three step explicit scheme is a more stable and accurate method compared with the conventional two-step scheme. The CFL condition of the three-step explicit scheme is 1·5 times larger than that of the conventional two-step scheme.
2. The three-step explicit solver applicable to an unstructured mesh has been successfully implemented on a massively parallel supercomputer.
3. As an example a large-scale computation of the tidal current in Tokyo Bay has been carried out. The simulation also accounted for the spread of a contaminant due to tidal flows.

From the results obtained in this paper, it can be concluded that the present method can be usefully applied to large-scale computations of various shallow water flow problems.

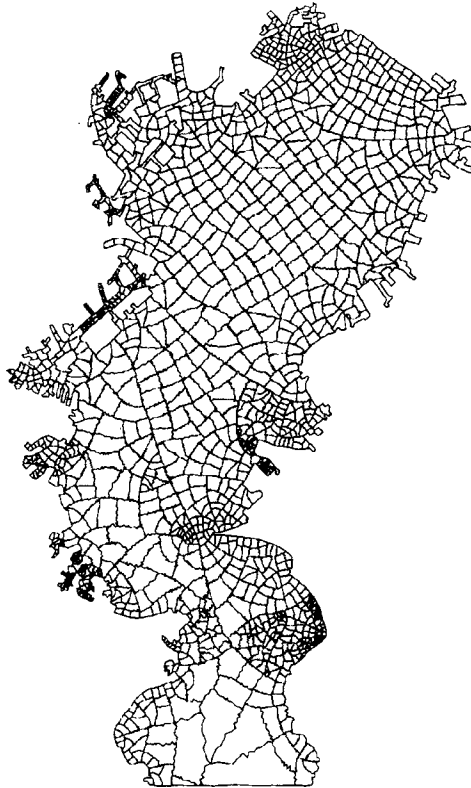Figure 7. Finite element discretization of Tokyo Bay
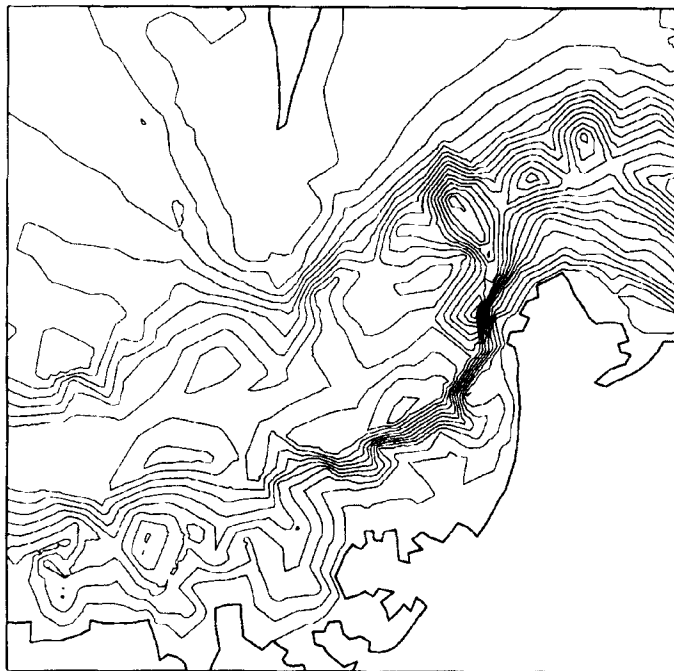
Figure 8. Mesh partitioning for 1024 vector units

Figure 9. Boundary and water depth diagram of Uraga–Suido channel
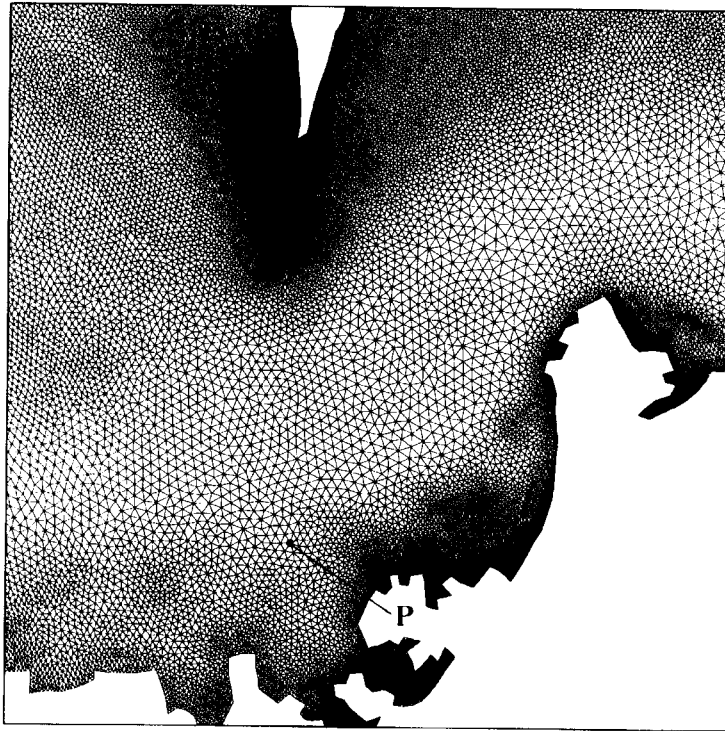
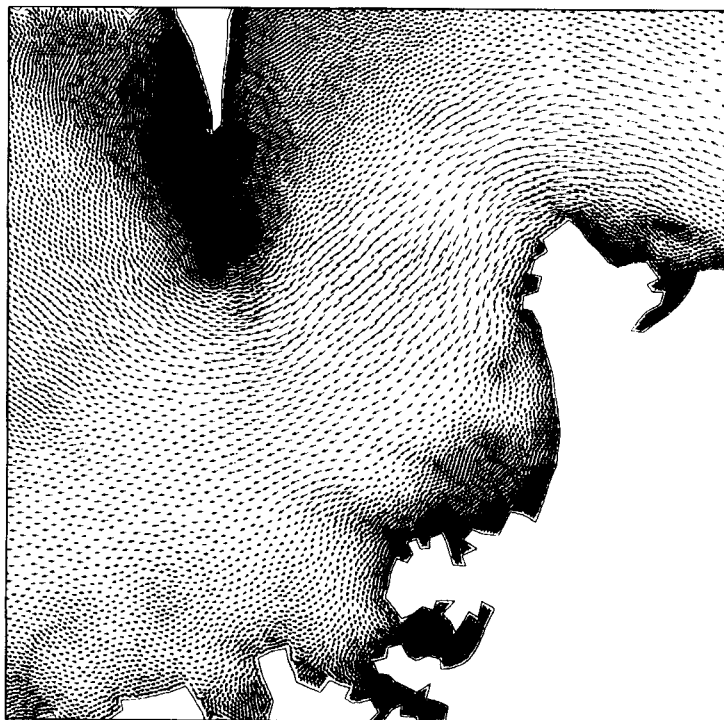Figure 10. Finite element discretization of Uraga–Suido channel

Figure 11. Computed current velocity at high tide
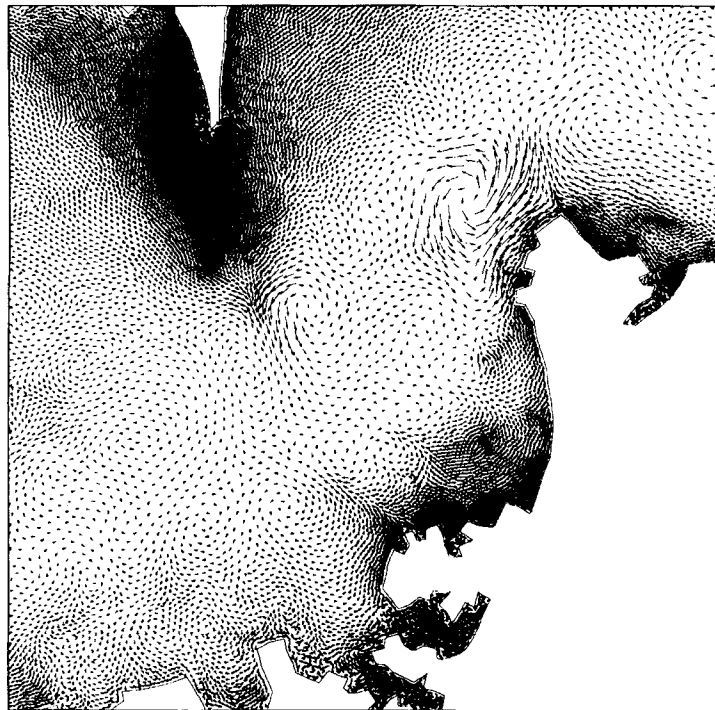
Figure 12. Computed current velocity at low tide

Figure 13. Computed residual current velocity
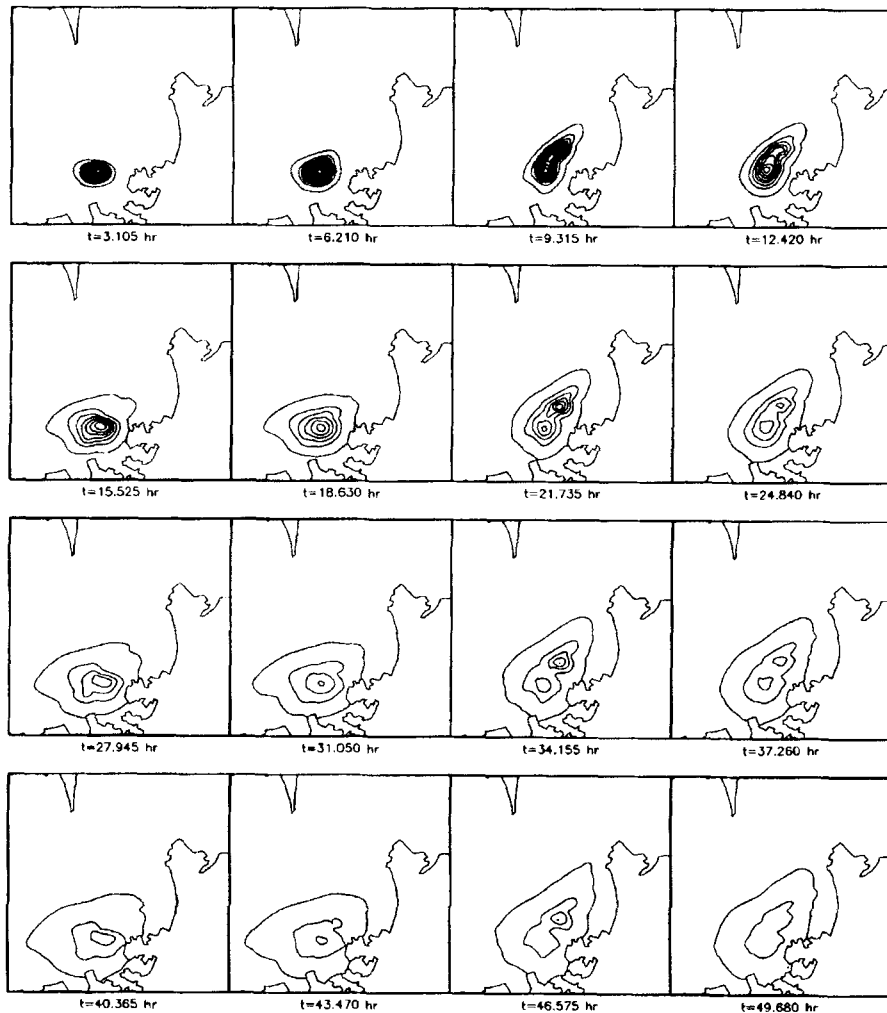
Figure 14. Streamline of residual flow

Figure 15. Computed contaminant spread at every 3·105 h

REFERENCES

1. T. E. Tezduyar, M. Behr, S. Mittal and A. A. Johnson, 'Computation of unsteady incompressible flows with the stabilized finite element methods—space–time formulations, iterative strategies and massively parallel implementations', in P. Smolinski, W. K. Liu, G. Hulbert and K. Tamma (eds), *New Methods in Transient Analysis*, AMD Vol. 143, ASME, New York, 1992, pp. 7–24.
2. M. Behr and T. E. Tezduyar, 'Finite element solution strategies for large-scale flow simulations', *Comput. Methods Appl. Mech. Eng.*, **112**, 3–24 (1994).
3. Z. Johan, K. K. Mathur, S. L. Johnsson and T. J. R. Hughes, 'An efficient communication strategy for finite element methods on the Connection Machine CM-5 system', *Comput. Methods Appl. Mech. Eng.*, **113**, 363–387 (1994).

4. M. Kawahara, H. Hirano, K. Tsubota and K. Inagaki, 'Selective lumping finite element method for shallow water flow', *Int. j. numer. methods fluids*, **2**, 89–112 (1982).

5. M. Kawahara and K. Kashiyama, 'Selective lumping finite element method for nearshore current', *Int. j. numer. methods fluids*, **4**, 71–97 (1984).

6. A. N. Brooks and T. J. R. Hughes, 'Streamline upwind/Petrov–Galerkin formulations for convection dominated flows with particular emphasis on the incompressible Navier–Stokes equations', *Comput. Methods Appl. Mech. Eng.*, **32**, 199–259 (1982).

7. T. E. Tezduyar and T. J. R. Hughes, 'Finite element formulations for convection dominated flows with particular emphasis on the Euler equations', *AIAA Paper 83-0125*, 1983.

8. C. B. Jiang, M. Kawahara, K. Hatanaka and K. Kashiyama, 'A three-step finite element method for convection dominated incompressible flow', *Comput. Fluid Dyn. J.*, **1**, 443–462 (1993).

9. P. Gresho, Personal communication, 1994.

10. M. Ichihara, T. Oomura, N. Fukusiro and R. Nozawa, 'An observation and simulation of tidal currents of Tokyo Bay', *Proc. 27th Natl. Conf. of Coastal Engineering*, JSCE, 1980, pp. 448–452.

11. K. Murakami, 'Numerical simulation of tidal currents by means of finite element method', *Tech. Note of Port and Harbor Research Institute (Ministry of Transport, Japan), No. 404*, 1981 (in Japanese).

12. T. Kodama and M. Kawahara, 'Multiple level finite element analysis for tidal current flow with non-reflective open boundary condition', *Proc. JSCE*, **446**, 89–99 (1992).

13. K. Kashiyama and T. Okada, 'Automatic mesh generation method for shallow water flow analysis', *Int. j. numer. methods fluids*, **15**, 1037–1057 (1992).

14. K. Kashiyama and M. Sakuraba, 'Adaptive boundary-type finite element method for wave diffraction–refraction in harbors', *Comput. Methods Appl. Mech. Eng.*, **112**, 185–197 (1994).

15. *Maritime Chart of Tokyo Datum, No. 90*, Marine Safety Agency, 1984.

16. *Harmonic Constant Table*, Marine Safety Agency, 1989.